







Turbulence hierarchy in foreign exchange markets

Giovani L. Vasconcelos ¹, Lucas R. C. Ribeiro ², Antônio M. S. Macêdo ²,
Iván R. R. González ^{2,3}, Raydonal Ospina ^{4,5} and Arthur A. Brum ⁶

¹*Departamento de Física, Universidade Federal do Paraná, Curitiba 81531-980, PR, Brazil*

²*Laboratório de Física Teórica e Computacional, Departamento de Física, Universidade Federal de Pernambuco, Recife 50670-901, PE, Brazil*

³*Instituto de Física, Facultad de Ciencias, Pontificia Universidad Católica de Valparaíso (PUCV), 23-40025 Valparaíso, Chile*

⁴*Departamento de Estatística, Universidade Federal da Bahia, Salvador 40170-110, BA, Brazil*

⁵*Departamento de Estatística, Universidade Federal do Pernambuco, Recife 50670-901, PE, Brazil*

⁶*Laboratório de Física Teórica e Computacional, Departamento de Física, Universidade Federal de Pernambuco, Recife 50670-901, PE, Brazil*



(Received 7 October 2023; accepted 12 March 2024; published 23 April 2024)

We present a multiscale stochastic analysis of foreign exchange rates using the H-theory formalism, which provides a hierarchical intermittency model for the information cascade in the currency market. We examine the distributions of returns and volatilities for the three most traded currency pairs: euro–U.S. dollar, U.S. dollar–Japanese yen, and British pound–U.S. dollar. We find that these markets have a hierarchy of timescales, with larger markets exhibiting more hierarchy levels. We provide a theoretical framework for understanding why the number of levels in the information cascade increases with market size, in analogy with similar behavior for the energy cascade in turbulence as a function of Reynolds number. We briefly argue that using turbulence-like models for financial markets can also provide valuable insights for developing efficient algorithmic trading strategies.

DOI: [10.1103/PhysRevE.109.044313](https://doi.org/10.1103/PhysRevE.109.044313)

I. INTRODUCTION

Turbulence is a ubiquitous phenomenon that transcends disciplinary boundaries, manifesting itself in various physical, biological, social, and even purely mathematical systems. Beyond its original context [1], turbulence-like behavior has been observed, for example, in disordered condensed matter systems, such as random lasers [2] and the integer quantum Hall transition [3], as well as in complex interdisciplinary systems, such as brain activity [4,5], seismic processes [6], and financial markets [7–12]. In many cases, however, the analogy with turbulence is largely tentative, as it stems from identifying certain common statistical features, such as power-law decay of the energy spectrum (akin to Kolmogorov’s famous 5/3 law) and scale-dependent probability distributions (associated with intermittency). In foreign exchange (forex) markets, on the other hand, a deep analogy between price fluctuations and fully developed turbulence has been proposed [7], whereby an “information cascade” (from longer to shorter timescales) among investors plays the role of the energy cascade (from larger to smaller length scales) in fluid turbulence. But, to date, confirmation of this hypothesis has been mostly indirect (e.g., via correlation between volatilities at different time horizons [13,14]). Here we present the first direct evidence of the presence of a hierarchy of timescales in forex markets, using a multiscale statistical mechanics formalism. Our findings suggest that the dynamics of forex markets can be modeled by means of a well-developed stochastic theory of turbulence [15], which may have deep implications for the understanding of the price formation process and the development of algorithmic trading strategies.

Forex is the most active and liquid financial market in the world, trading several trillion U.S. dollars per day [16]. It is a platform open 24 h a day, 5 days a week, where anyone can trade from anywhere in the world, thus representing a truly global market with a multitude of investors, from single individuals to large financial institutions. Interestingly, an asymmetric flow of information from long-term to short-term traders has been observed in this market [13]. These characteristics suggest a natural analogy between forex price fluctuations and velocity fluctuations in fully developed turbulence [7].

In this article, we investigate the turbulent nature of three most traded currency pairs, namely euro and U.S. dollar (EUR-USD), British pound and U.S. dollar (GBP-USD), and U.S. dollar and Japanese yen (USD-JPY), which together represent more than half of the total trading volume. We have analyzed 1-h quotes from November 2012 to April 2023 [17], corresponding to about 64 000 points for each currency pair, as show in Fig. 1. The challenge is to extract from these random-walk-like time series more precise information about the underlying complex dynamical process that leads to price fluctuations. To address this challenge, we have developed an intermittency model for the information cascade in forex markets. Our approach is based on a stochastic hierarchical formalism (H theory), which was first developed in the context of fluid turbulence [18,19] and has since been successfully applied to various other systems [2,3,15]. H theory yields a family of probability distributions labeled by the number, N , of levels in the cascade hierarchy. Comparing the model to the empirical data allows us to estimate the number of effective

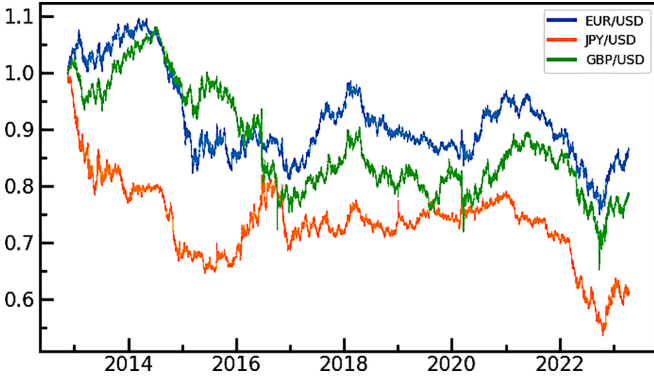


FIG. 1. One-hour quotes for the exchange rates of the three most traded currency pairs: EUR-USD (blue), JPY-USD (orange), and GBP-USD (green). Here we have normalized the initial point of all three series to unity for convenience of visualization.

timescales within each currency market. The ordering of the forex markets from higher to lower N predicted by the theory is in complete agreement with the ranking of the currency pairs according to trading volume. Our results, thus, not only reveal direct evidence of a turbulence-like hierarchical dynamical structure within forex markets but also show that the more active a market is, the greater the number of levels in the underlying information cascade.

The paper is organized as follows. In Sec. II, we present our stochastic volatility hierarchical model (Sec. II A), discuss the main properties of the resulting stationary distribution of returns (Sec. II B), and introduce a joint fitting procedure to fit simultaneously the empirical data for *both* returns and volatilities (Sec. II C). The results of the application of our approach to the three most traded currency pairs, namely EUR-USD, GBP-USD, and USD-JPY, are presented in Sec. III, while in Sec. IV we briefly discuss the relevance and implications of our results. Finally, our main findings and conclusions are summarized in Sec. V.

II. METHODOLOGY

A. The model

We model the logarithmic return of exchange rates, $x_\tau(t) = \ln S(t + \tau) - \ln S(t)$, where $S(t)$ is the rate of a given currency pair at time t and τ is a short timescale, by the following Langevin equation:

$$dx_\tau(t) = -\mu x_\tau(t)dt + \sqrt{\mu v_\tau(t)}dW_0(t), \quad (1)$$

where μ is a positive constant, $v_\tau(t)$ is the volatility at scale τ , and $W_0(t)$ is a Wiener process (standard Brownian motion). Empirical studies have long shown that volatility of financial prices not only varies in time [20] but also exhibits clustering across timescales [21]—a phenomenon analogous to the intermittency of energy dissipation in turbulence. In forex markets, in addition, there is evidence of an asymmetric flow of information from long to short timescales, meaning that volatility measured at short time horizons is impacted by long-horizon volatility [13,14], but not vice versa—a process akin to the energy cascade in turbulence.

Thus, in the spirit of Kolmogorov's theory of intermittency [1], we model the information cascade in forex markets by the following system of stochastic differential equations for the scale-dependent volatilities [15]:

$$dv_i(t) = -\gamma_i[v_i(t) - v_{i-1}(t)]dt + \kappa_i v_i(t)dW_i(t), \quad (2)$$

$$i = 1, \dots, N,$$

where γ_i and κ_i are positive constants and $W_i(t)$ are independent Wiener processes. Here we assume a hierarchy of timescales, $\tau_i \ll \tau_{i-1}$, $i = 1, \dots, N$, so that v_i is the volatility at scale τ_i , with τ_0 representing the largest timescale (say, the span of the time series) and v_0 being the historical volatility (i.e., measured at scale τ_0). The deterministic term in (2) captures the asymmetric flow of information from higher to lower levels down the hierarchy, while the multiplicative noise term ensures that volatility fluctuates but remains always positive [15]. The volatility appearing in (1) is associated with the volatility at the smallest scale in the hierarchy, i.e., $v(t) = v_N(t)$. We also note that by taking the mean of (2), one can readily show that in the stationary regime the variables v_i all have the same mean $\langle v_i \rangle = v_0$, for $i = 1, \dots, N$. In essence, this implies that the distinct volatilities across various timescales fluctuate around the same mean, namely the historical volatility v_0 .

Many stochastic volatility (SV) models have been used in finance [20], including econometric-based models, such as GARCH and HARCH models [22], among others. Our stochastic hierarchical model defined by (1) and (2) has the advantage that it describes explicitly the different horizon volatilities and yet admits, under reasonable approximations, an analytical solution for both the return and volatility distributions which describe remarkably well the empirical data; see below. Also, because our model for the stochastic volatility dynamics is formulated hierarchically, it allows us to probe the number of effective timescales (i.e., levels in the hierarchy) present in a given dataset—a property that is not easily accessible in other SV models. In our formulation above we have assumed that the Wiener processes driving returns and volatilities are uncorrelated, i.e., $\langle dW_i(t)dW_j(t) \rangle = dt\delta_{ij}$, $i, j = 0, 1, \dots, N$. In a more general setting we could allow, for instance, for correlation between returns and the short-term volatilities, i.e., $\langle dW_0(t)dW_N(t) \rangle = \rho dt$, with $\rho < 0$, so as to capture the so-called *leverage effect*, which pertains to the often found negative correlation between asset prices or returns and volatilities [23,24]. Since here we are mainly interested in the long-term distribution of returns and volatilities, such correlation effects are not relevant for our purposes.

Because the model composed of (1) and (2) is not exactly soluble, we appeal to the separation of timescales to obtain an approximate analytical solution. First, it is clear that the volatility $v_N(t)$ in (1) varies more slowly than the returns $x(t)$, that is, $\tau_N \gg \tau$, since the former is an aggregate quantity of the latter. Thus, over a scale of time τ_N , during which the volatility $v_N(t)$ does not vary much, the returns will tend to reach a quasistationary regime described by a Gaussian distribution with variance v_N :

$$P(x|v_N) = \frac{1}{\sqrt{2\pi v_N}} \exp\left(-\frac{x^2}{2v_N}\right). \quad (3)$$

Compounding this Gaussian over all possible values of v_N , we can write the probability distribution, $P(x_\tau)$, of returns as

$$P(x_\tau) = \int_0^\infty \frac{1}{\sqrt{2\pi v_N}} \exp\left(-\frac{x_\tau^2}{2v_N}\right) f(v_N) dv_N, \quad (4)$$

where $f(v_N)$ is the stationary probability density function of $v_N(t)$.

In the same vein, we solve (2) by holding the slower variable v_{i-1} fixed and computing the stationary solution, $f(v_i|v_{i-1})$, of the corresponding Fokker-Planck equation, which yields an inverse-gamma distribution:

$$f(v_i|v_{i-1}) = \frac{(\beta_i v_{i-1})^{\beta_i+1}}{\Gamma(\beta_i+1)} v_i^{-\beta_i-2} \exp\left(-\frac{\beta_i v_{i-1}}{v_i}\right), \quad (5)$$

where $\beta_i = 2\gamma_i/\kappa_i^2$. The distribution $f(v_N)$ at the smallest scale is then obtained by integrating over the larger scales. More specifically, we first write $f(v_N) = \int f(v_N|v_{N-1})f(v_{N-1})dv_{N-1}$ and then use this expression recursively up to the top level of the hierarchy:

$$f(v_N) = \int dv_{N-1} \dots \int dv_1 \prod_{i=1}^N f(v_i|v_{i-1}). \quad (6)$$

Inserting (5) into (6) and performing this multiple integral yields the following expression [15]:

$$f(v_N) = \frac{1}{v_0 \omega \Gamma(\beta+1)} G_{N,0}^{0,N} \left(\begin{matrix} -\beta-1 \\ - \end{matrix} \middle| \frac{v_N}{v_0 \omega} \right), \quad (7)$$

where $\omega = \prod_{j=1}^N \beta_j$, $\beta \equiv (\beta_1, \dots, \beta_N)$, $\Gamma(\beta) \equiv \prod_{j=1}^N \Gamma(\beta_j)$, and $G_{p,q}^{m,n}$ is the Meijer G function [25].

Now, substituting (7) into (4), one obtains (see details of derivation in the next section)

$$P_N(x) = \frac{1}{\sqrt{2\pi \omega v_0}} \frac{\Gamma(\beta+3/2)}{\Gamma(\beta+1)} {}_N F_0 \left(\beta+3/2; -\frac{x^2}{2\omega v_0} \right), \quad (8)$$

where ${}_p F_q$ is the generalized hypergeometric function. In the remainder of the paper, we will set $\beta_i = \beta$, $i = 1, \dots, N$, which is justifiable if we assume scale invariance across the information hierarchy, so that the conditional volatility distributions $f(v_i|v_{i-1})$ have the same form at all levels of the hierarchy. From the asymptotic behavior of the function ${}_N F_0(\mathbf{a}, x)$, see below, one can show that the distributions $P_N(x)$ have *power-law tails*:

$$P_N(x) \approx \frac{C_N}{x^{2\beta+3}}, \quad |x| \rightarrow \infty, \quad (9)$$

for some constant C_N that increases with N ; see below. We also note that by construction $P_N(x)$ has zero mean, $\langle x \rangle = 0$, and finite variance, $\langle x^2 \rangle = v_0$. As discussed elsewhere [15], there is a second class of intermittency models that leads to distributions, $P_N(x)$, with stretched exponential tails. Here, however, we shall consider only the power-law distributions presented above, as this class proved more suitable for forex data. In the next section we give more details about the derivation of Eq. (8) and also discuss some relevant properties of this class of power-law-tailed distributions.

B. The power-law distribution class

In order to obtain Eq. (8), we first insert (7) into (4), which yields

$$P(x_\tau) = \int_0^\infty \frac{1}{\sqrt{2\pi v_N}} \exp\left(-\frac{x_\tau^2}{2v_N}\right) \frac{1}{v_0 \omega \Gamma(\beta+1)} \times G_{N,0}^{0,N} \left(\begin{matrix} -\beta-1 \\ - \end{matrix} \middle| \frac{v_N}{v_0 \omega} \right) dv_N. \quad (10)$$

Expressing the exponential as a Meijer G function,

$$\exp(ax) = G_{0,1}^{1,0} \left(\begin{matrix} - \\ 0 \end{matrix} \middle| -ax \right), \quad (11)$$

and making use of integration properties of the product of two G functions [25], it is straightforward to integrate analytically (10), yielding:

$$P_N(x) = \frac{1}{\sqrt{2\pi \omega v_0} \Gamma(\beta+1)} G_{N,1}^{1,N} \left(\begin{matrix} -\beta-1/2 \\ 0 \end{matrix} \middle| \frac{x^2}{2\omega v_0} \right). \quad (12)$$

Now, using the identity

$${}_p F_q \left(\begin{matrix} \mathbf{a}_p \\ \mathbf{b}_q \end{matrix} \middle| z \right) = \frac{\Gamma(\mathbf{b}_q)}{\Gamma(\mathbf{a}_p)} G_{p,q+1}^{1,p} \left(\begin{matrix} 1-\mathbf{a}_p \\ 0, 1-\mathbf{b}_q \end{matrix} \middle| -z \right), \quad (13)$$

where ${}_p F_q$ is the generalized hypergeometric function, it then follows that $P_N(x)$ can be expressed more simply as

$$P_N(x) = \frac{1}{\sqrt{2\pi \omega v_0}} \frac{\Gamma(\beta+3/2)}{\Gamma(\beta+1)} {}_N F_0 \left(\beta+3/2; -\frac{x^2}{2\omega v_0} \right), \quad (14)$$

thus obtaining Eq. (8).

The case $N = 1$ is of particular interest because the distribution in (14),

$$P_1(x) = \frac{1}{\sqrt{2\pi \beta v_0}} \frac{\Gamma(\beta+3/2)}{\Gamma(\beta+1)} {}_1 F_0 \left(\beta+3/2; -\frac{x^2}{2\beta v_0} \right), \quad (15)$$

can be expressed in terms of a simpler function using the identity ${}_1 F_0(a, z) = (1-z)^{-a}$ [25], which yields

$$P_1(x) = \frac{1}{\sqrt{2\pi \beta v_0}} \frac{\Gamma(\beta+3/2)}{\Gamma(\beta+1)} \left(1 + \frac{x^2}{2\beta v_0} \right)^{-(\beta+\frac{3}{2})}. \quad (16)$$

Alternatively, $P_1(x)$ can be written in terms of the so-called q -Gaussian distribution [26,27]:

$$P_1(x) = \frac{\sqrt{q-1}}{\sqrt{(5-3q)\pi\sigma^2}} \frac{\Gamma(\frac{1}{q-1})}{\Gamma(\frac{1}{q-1}-\frac{1}{2})} \exp_q \left[-\frac{x^2}{(5-3q)\sigma^2} \right], \quad (17)$$

where

$$q = 1 + \frac{2}{2\beta+3}, \quad (18)$$

$\sigma^2 = v_0 = \langle x^2 \rangle$, and

$$\exp_q(x) \equiv [1 + (1-q)x]^{1/q}. \quad (19)$$

Relation (18) implies that $1 < q < \frac{5}{3}$, since $\beta > 0$ by definition. This upper bound ensures a finite second moment for

the q -Gaussian distribution in (17). The q -Gaussian has been widely used to model distributions with fat tails, especially in the context of nonextensive statistical mechanics, where the q -exponential distribution is obtained from maximizing a generalized entropy functional [27]. Notably, the emergence of the q -Gaussian distribution in H theory does not rely on the formalism of nonextensive statistical mechanics. Rather, it emerges as the first member of a family of non-Gaussian, power-law-tailed distributions which arises from an underlying hierarchical stochastic dynamics, as discussed in Sec. II A.

For $N = 1$ the distribution $P_1(x)$ has an explicit algebraic form, see (16), and hence a power-law decay for large x :

$$P_1(x) \sim \frac{1}{x^{2\beta+3}}, \quad x \gg x_1^* = \sqrt{2\beta v_0}. \quad (20)$$

Now, from the asymptotic behavior of the function ${}_N F_0$,

$${}_N F_0(a_1, \dots, a_N; -x) \sim \sum_{i=1}^N c_i x^{-a_i} \left[1 + O\left(\frac{1}{x}\right) \right], \quad \text{for } |x| \rightarrow \infty, \quad (21)$$

where the c_i 's are constants, it follows that the distributions in (8) all have power-law tails for any N . In particular, under the assumption of identical β_i , that is, $\beta_i = \beta, i = 1, \dots, N$, the distributions $P_N(x)$ all have the *same power-law tail*:

$$P_N(x) \approx \frac{C_N}{x^{2\beta+3}}, \quad \text{for } |x| \gg x_N^*, \quad (22)$$

for some constant C_N and some characteristic scale x_N^* . One thus sees that Eq. (14), with $\beta_i = \beta$, provides a large class of different distributions but all having the same power-law tail exponent (for fixed β).

One important point to bear in mind, however, is that both the constant C_N and the characteristic value x_N^* in (22) increase with N . This means that the greater the N , the more delayed (i.e., for larger values of x) is the start of the power-law regime. This is illustrated in Fig. 2(a), which shows plots of the function $P_N(x)$ given in (14), for $N = 1, 2, 3, 4, 5$ and $v_0 = \beta = 1$, so that all distributions have unity variance and the same power-law tail. In Fig. 2(b) we plot in log-log scale the positive parts (i.e., for $x > 0$) of the distributions shown in Fig. 2(a), where one sees that the tails tend to become parallel for large x , but the crossover to the power-law regime (which appears in the log-log plot as a straight downward line) is considerably delayed as N increases. Note furthermore that, although the distributions have the same power-law tail in the very large x limit, they differ significantly in the central region, as seen in Fig. 2(a). Conversely, if one requires that the distributions $P_N(x)$ have, for different N 's, comparable behavior in a (small) finite region near the center of the distribution, then the respective values of β must necessarily increase with N to compensate the fact that C_N increases with N , then leading to quite different tail behaviors for large x .

The previous discussion thus shows that caution is needed when fitting empirical data (which usually have limited range) with theoretical power-law distributions: Fitting the tail may lead to quite different behavior in the center and vice versa. Furthermore, as shown above and also discussed elsewhere [28,29], distributions of the measured signal (say, returns in financial data or velocity increments in turbulence) can be

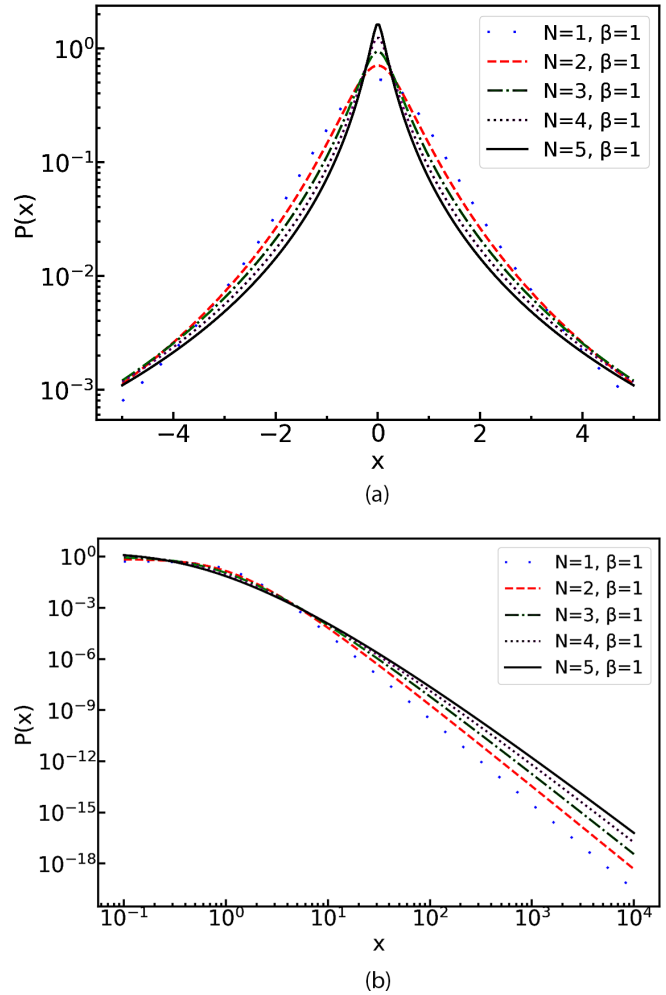


FIG. 2. (a) Plots of the distribution $P_N(x)$ given in Eq. (12) for $v_0 = 1, \beta = 1$, and $N = 1, 2, 3, 4, 5$. (b) Same as in (a) in log-log scale for the positive side ($x > 0$) of the distributions.

fitted reasonably well by different model distributions, thus making it difficult to select between competing models. In other words, model selection on the basis solely of the signal distribution tends to be less discriminating, because different theoretical curves can yield somewhat comparable results especially for limited datasets. To circumvent this limitation, we propose a joint fitting procedure (see below) where we undertake to fit *simultaneously* the empirical distributions of both the signal (returns) and its background (volatilities), using the respective formulas predicted by our model. We emphasize that this is a more stringent procedure than simply fitting the return data, because it tests both the model distribution and the assumptions that went into deriving the model.

C. The volatility series and the joint fit procedure

As indicated above, since we have analytical expressions for both the return and volatility distributions, we can fit the two theoretical curves, Eqs. (8) and (7), simultaneously to the empirical histograms for returns and volatilities, respectively. To do this, we first construct a volatility series $\{v(t)\}$ for a given empirical return series $\{x_\tau(t)\}$, as described below.

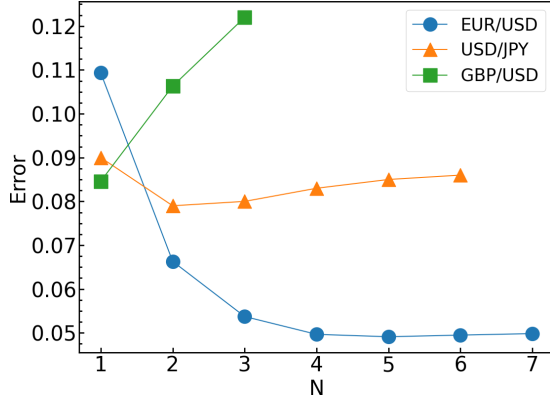


FIG. 3. Errors of the joint fit as a function of the number N of hierarchy levels for the three most traded currency pairs: EUR-USD (blue circles), USD-JPY (orange triangles), and GBP-USD (green squares).

We start by considering a moving window of size M over the original time series $x(t)$ and for each such window we compute a variance estimator, $v(t) = \frac{1}{M-1} \sum_{j=0}^{M-1} [x(t - j\delta t) - \bar{x}(t)]^2$, where $\bar{x}(t) = \frac{1}{M} \sum_{j=0}^{M-1} x(t - j\delta t)$. This process generates a new time series $v_M(t)$. Next, we numerically compound a Gaussian with the empirical distribution of the series $v_M(t)$, as indicated in (4), where the integral can be computed simply as a sum:

$$P^{(M)}(x) = \frac{1}{n-M} \sum_{i=1}^{n-M} \frac{1}{\sqrt{2\pi v_M(i)}} \exp\left[-\frac{x^2}{2v_M(i)}\right], \quad (23)$$

where n is the number of points in the original series $x(t)$. We repeat this for various M and select the optimal value M^* for which the corresponding compound distribution $P^{(M)}(x)$ best fits the empirical distribution of the original series.

Once the optimal window size, M^* , is obtained we then perform a joint fit of the two theoretical distributions $P_N(x)$ and $f_N(v)$, see Eqs. (8) and (7), to the signal data, $x(t)$, and the auxiliary background series, $v_{M^*}(t)$, respectively. More precisely, for a given N , we determine the parameter β that minimizes the following joint error function:

$$\text{Error}(N) = \frac{1}{2n - M^*} \left[\sum_{i=1}^n |\ln P_N(x_i) - \ln P_i| + \sum_{i=1}^{n-M^*} |\ln f_N(v_i) - \ln f_i| \right], \quad (24)$$

where P_i and f_i are the corresponding empirical values of the distributions (histograms) of returns and volatilities, respectively. We emphasize that for a given N we only need to perform a one-parameter joint fit to the data to find the best β , for we have set $v_0 = 1$, since the empirical distributions are normalized to unit variance. For a given dataset, we perform the joint fit procedure for different values of N and then select the best N as that for which the above error function is minimum. Note that fixing a value of N means that the volatility hierarchy is considered up to that value, i.e., we have $i = 1, 2, \dots, N$ in Eq. (2); see also Eq. (6). Thus, as we increase N , we increase the depth of the hierarchy. We proceed

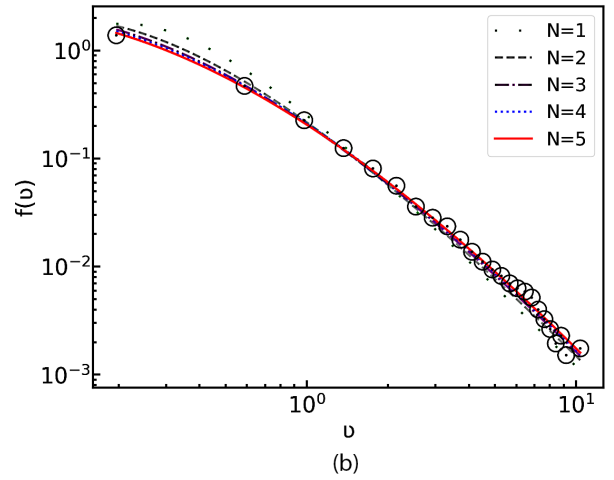
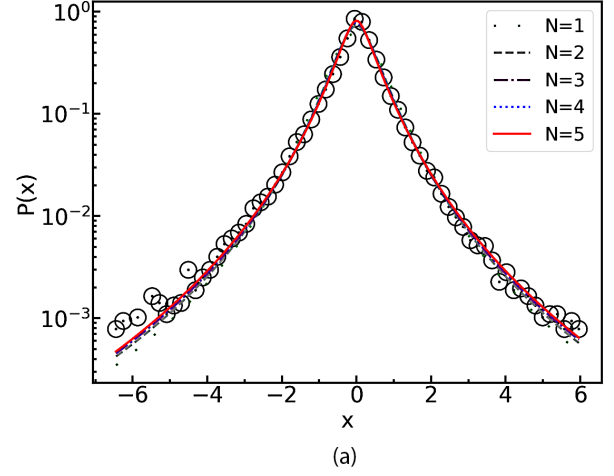


FIG. 4. (a) Distribution of exchange rates returns (black circles) for EUR-USD and the H-theory prediction (lines) for $N = 1$ and $\beta = 0.53$ (green dashed), $N = 2$ and $\beta = 0.93$ (orange dotted), $N = 3$ and $\beta = 1.36$ (purple dashed), $N = 4$ and $\beta = 1.85$ (blue dashed), and $N = 5$ and $\beta = 2.27$ (red). Here the best joint fit was attained for $N = 5$; see Fig. 3. (b) Histogram (black circles) of the volatility series $v(t)$ and model prediction (lines) with the same parameters and colors convention as in (a).

in this manner until we obtain the optimal N for which the joint fit gives the smallest error. In the next section we show the results of the joint fit procedure as applied to the three datasets considered here.

III. RESULTS

In Fig. 3 we show plots of the error function (24) as function of N for the three currency pairs considered here. From this figure, we find that the minimum error for the EUR-USD pair is attained at $N = 5$, whereas for USD-JPY the minimum error happens at $N = 2$. For the GBP-USD pair, however, the error increases with N and hence we consider $N = 1$ to be the best value (i.e., smallest error).

In Fig. 4 we show the results of the joint fits of the distributions of returns and volatilities for the EUR-USD prices for $N = 1, 2, 3, 4, 5$, in which case we have found that the smallest error was attained for $N = 5$, as just mentioned, and

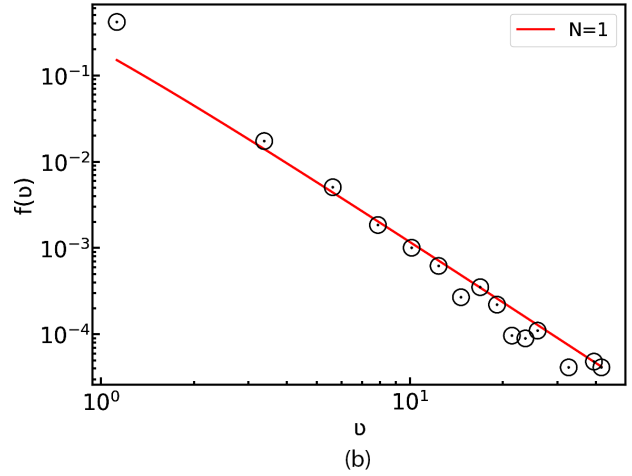
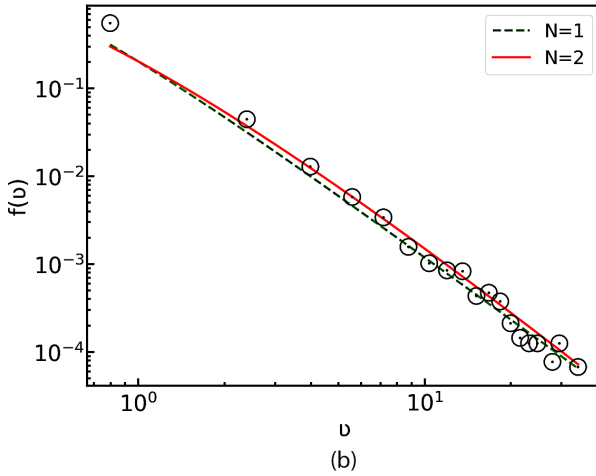
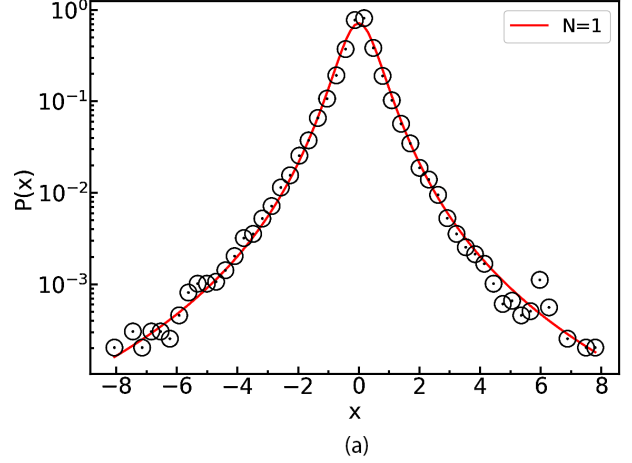
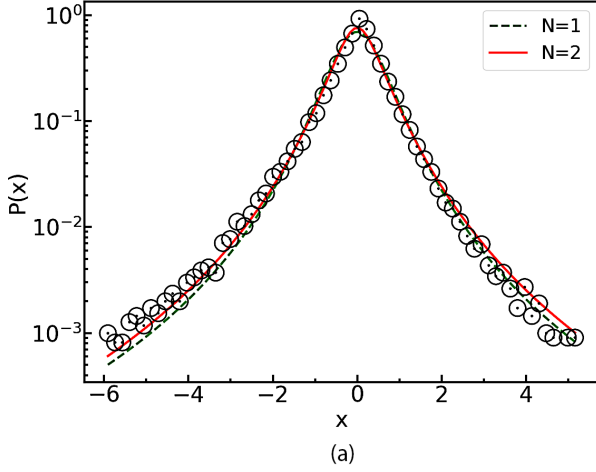


FIG. 5. (a) Distribution of exchange rates returns (black circles) for USD-JPY and the H-theory prediction (lines) for $N = 1$ and $\beta = 0.38$ (green dashed) and $N = 2$ and $\beta = 0.85$ (red). Here the best joint fit was attained for $N = 2$; see Fig. 3. (b) Histogram (black circles) of the volatility series $v(t)$ and model prediction (lines) with the same parameters and colors convention as in (a).

FIG. 6. (a) Distribution of exchange rates returns (black circles) for GBP-USD and the H-theory prediction (red line) for $N = 1$ and $\beta = 0.35$. Here the best joint fit was attained for $N = 1$; see Fig. 3. (b) Histogram (black circles) of the volatility series $v(t)$ and model prediction (line) with the same parameters and colors convention as in (a).

$\beta = 2.27$. Here the lines represent the corresponding theoretical curves for each N , while the circles correspond to the empirical histograms. The agreement between theory and data for the best fit, i.e., $N = 5$ (red solid lines), is excellent for both the return [Fig. 4(a)] and the volatility [Fig. 4(b)] distributions. In particular, note that the theoretical curve for $N = 5$ fits remarkably well the empirical return distribution in all its extension—from the center to the tails. One can also see that as N increases the agreement between the theoretical curves and the data visibly improves—both at the center and at the tails of the distributions—until the best fit among them is reached for $N = 5$.

In Fig. 5 we show the corresponding best joint fits for the USD-JPY pair for $N = 1$ and for $N = 2$, where the best fit occurred for the latter value with $\beta = 0.85$; see Fig. 3. Here again we find a very good agreement between the theoretical curves and the data for the best fit case ($N = 2$, red solid curves), except perhaps on the right tail of the return distribution [Fig. 5(a)] owing to the data skewness; see below for further discussion of this effect. In Fig. 6 we show the fit

results for the GBP-USD data, where the best fit occurred for $N = 1$ and $\beta = 0.35$, in which the case the distribution $P_N(x)$ reduces to the q -Gaussian distribution; see (17). As discussed in Sec. II B, the q -Gaussian is but the first member of a hierarchical family of power-law distributions. Thus, when seeking to apply power-law tailed distributions to a specific system, it is prudent to test the data against different distributions within that class, to decide which value of N best suits the data. In our study, we found that the q -Gaussian ($N = 1$) was the best choice for only one dataset (GBP-USD).

IV. DISCUSSION

We have seen above that the three most active forex markets are ranked by our theory in the same order, according to the number N of timescales, as follows: EUR-USD (28% of trading volume) with $N = 5$; USD-JPY (13% of trading volume) with $N = 2$; and GBP-USD (11% of trading volume) with $N = 1$. These findings show that the hierarchy depth increases with market size, an interesting result that demands further discussion.

Information cascades in financial markets are believed to arise because traders have different investment horizons, which in turn affect their investment strategies [13]. Long-term traders watch the market much less frequently than short-time traders and hence the former's investment decisions are not much affected by short-horizon volatility. Conversely, for short-term traders the level of coarse volatility matters more because it might reveal trading opportunities. Thus, volatilities measured at different time horizons tend to reflect the perceptions and actions of different market components [13]. In other words, the existence of investors with different investment horizons naturally leads to different timescales within the volatility dynamics, whereby longer-horizon volatilities affect the shorter-term volatilities but usually not the other way around. Because volatility in financial markets can be viewed as a measure of information, this asymmetry in the information flow is interpreted as an information cascade from larger to smaller timescales [30]. What is less clear, however, is how to estimate the number of relevant timescales in a given dataset for a given market.

In fluid dynamics, the nature of a fluid flow (whether laminar or turbulent) is characterized by the Reynolds number, Re , which is a dimensionless parameter defined by the ratio of inertial and viscous forces, $Re = LU/\nu$, where L is a characteristic length scale, U is the mean flow velocity, and ν is the kinematic viscosity [1]. Fully developed turbulence appears for high Reynolds numbers. In the turbulent regime, the existence of typical large (integral) and small (dissipation) timescales can help to estimate the number of levels in the energy cascade [19], with the separation between the largest and smallest scales increasing with Reynolds number [1]. For example, in an application of H theory to Lagrangian turbulence, on using the integral timescale, T_L , and the Kolmogorov timescale, τ_η , it was possible to relate the number N of scales to the Taylor-scale Reynolds number as $N = \log_2(T_L/\tau_\eta) = \log_2(R_\lambda/\sqrt{15})$, which was found in good agreement with the N obtained from fitting the data [19]. (An analogous argument was made in a recent application of H theory to the magnetoconductance fluctuations in the quantum Hall transition, where N was also estimated as the log-ratio of the system size and the lattice spacing [3].)

Similar concepts are more elusive in financial markets, but some attempts have been made to render the “map” between fluid turbulence and financial markets more quantitative [7–12,31], including the notion of a “Reynolds number” for foreign exchange rates [31]. In the context of forex trading, which is our main focus here, one is led to consider the market size, say, in trading volume, as a measure of the corresponding integral scale since no other obvious characteristic large scale is present in such global electronic market. It is also reasonable to expect that the larger (i.e., more active) a market is, the larger the spread of investment horizons within that market, so that more active markets should have a larger number of relevant timescales (when comparing quotes at the same short time resolution). This hypothesis is in line with our result that the largest forex market (EUR-USD) has the largest number of timescales ($N = 5$), as identified by our model, whereas the second most traded currency pair, namely USD-JPY, was found to have $N = 2$. Indeed, it is worthy

of note that the size of the EUR-USD market is about 2.2 times that of the USD-JPY market, which is roughly the same ratio (namely, 2.5) as between the respective N 's in these two markets, thus lending further support to our model. The same proportion does not hold when comparing the USD-JPY ($N = 2$) and GBP-USD ($N = 1$) markets, as the former is only about 20% larger than the latter. One possible source of this discrepancy in the fact that our hierarchical cascade is “discrete,” in the sense that N varies only in steps of 1. (Some continuous cascade models have been proposed for turbulence and financial markets [32,33], and it would be interesting to generalize our hierarchical model in this direction in the future.) Also, other economic factors besides market size might affect the number of relevant timescales. For example, it is clear from visual inspection of Fig. 1 that the GBP-USD quotes tend to follow similar patterns of fluctuations as the EUR-USD pair, which is perhaps expected on the basis of the close economic ties between the United Kingdom and the euro zone, particularly before Brexit. This might imply in turn that traders do not need to watch the GBP-USD as frequently, as some information about this market can perhaps be inferred from the EUR-USD prices, thus further reducing the number of effective timescales in the former, as our model predicts. In summary, although further studies are necessary to more firmly establish our hypothesis above—namely that the number of timescales in forex markets increases with market size—this relationship is well supported by the results reported here, where the three most traded currency pairs are ranked by our model in precisely the same ordering according to the number N of scales.

Our results open up interesting new avenues of research, some of which we briefly discuss below. First, we note that the analysis presented here was limited to the three most traded currency pairs, where we saw that the third most active pair (GBP-USD) already gave the least number ($N = 1$) of hierarchy levels. It would therefore be interesting to test our hypothesis—namely, that N increases with market size—in other markets, such as equity markets and stock exchange indexes.

Besides the information cascade, another interesting stylized fact in financial data with a counterpart in turbulence is the negative asymmetry of return distributions, which is analogous to the negative skewness of velocity increments in turbulent flows. In turbulence, negative skewness follows from Kolmogorov's famous 4/5 law [1]. There is, however, no similar theoretical underpinning for the asymmetry of returns in forex markets. Negative skewness in financial data is often attributed to the investors' tendency to react more strongly to losses (“bad news”) than to gains (“good news”) [34], but this argument does not quite apply to exchange rates which have higher symmetry [23]. Indeed, all three datasets analyzed here display a small but noticeable degree of asymmetry, as can be seen in Figs. 4(a), 5(a), and 6(a). The asymmetry in forex markets thus seems to be an intrinsic dynamic feature of the information cascade. Recently, an extended version of the H theory was introduced to model asymmetric distributions in turbulence [29] and its application to forex data will be investigated in the future.

Another important stylistic fact of financial data is the so-called *leverage effect*, which refers to the negative correlation

between asset returns and return volatilities. As mentioned in Sec. II A, correlation between returns and volatilities can be introduced in our model by considering correlated Brownian motions in the respective EDEs. This was not done in the present paper because it was not relevant for our purposes here, but it is an interesting avenue of research that could be worth pursuing.

V. CONCLUSION

We have analyzed the “turbulent” nature of foreign exchange markets and found direct evidence of a hierarchy of timescales in currency market dynamics. More specifically, we have estimated the number of effective timescales in the three most traded currency pairs, namely EUR-USD, USD-JPY, and GBP-USD, using the intermittency model of H theory. Our results show that the larger the currency market, the greater the number of relevant timescales, in direct analogy with turbulence where the separation between the largest and the smallest scales in the energy cascade increases with Reynolds number.

Our approach sheds new light into the complex process of how information, as measured by price volatility, cascades down from longer to shorter timescales. Understanding the hierarchical dynamics of exchange rates using turbulence-like

models, as done in the present study, is also of practical importance for it can provide deeper insights into developing efficient algorithmic trading strategies. More specifically, the H-theory approach to modeling the price and volatility dynamics for a given forex pair can be used to estimate its local trend and volatility level, which could inform buy-sell decisions in a trading algorithm. Additionally, our approach draws inspiration from the use of analog physical systems, such as hydrodynamic simulations of black hole physics [35], to gain insights into complex phenomena, demonstrating the potential of interdisciplinary approaches in advancing our understanding of financial markets.

ACKNOWLEDGMENTS

This work was supported in part by the following Brazilian agencies: Conselho Nacional de Desenvolvimento Científico e Tecnológico (CNPq), under Grants No. 312985/2020-7 (GLV), No. 307626/2022-9 (AMSM), No. 303192/2022-4, and No. 402519/2023-0 (R.O.) and Grant No. 167348/2018-3 (A.A.B.), and Coordenação de Aperfeiçoamento de Pessoal de Nível Superior (CAPES). Agencia Nacional de Investigación y Desarrollo (ANID, Chile) is also acknowledged for the grant received by I.R.R.G (ALMA-ANID Project No. 31220004).

-
- [1] U. Frisch, *Turbulence: The Legacy of A. N. Kolmogorov* (Cambridge University Press, Cambridge, UK, 1995).
 - [2] I. R. R. González, B. C. Lima, P. I. R. Pincheira, A. A. Brum, A. M. S. Macêdo, G. L. Vasconcelos, L. de S. Menezes, E. P. Raposo, A. S. L. Gomes, and R. Kashyap, *Nat. Commun.* **8**, 15731 (2017).
 - [3] A. L. R. Barbosa, T. H. V. de Lima, I. R. R. González, N. L. Pessoa, A. M. S. Macêdo, and G. L. Vasconcelos, *Phys. Rev. Lett.* **128**, 236803 (2022).
 - [4] G. Deco and M. L. Kringelbach, *Cell Rep.* **33**, 108471 (2020).
 - [5] G. Deco, S. Liebana Garcia, Y. Sanz Perl, O. Sporns, and M. L. Kringelbach, *Commun. Phys.* **6**, 74 (2023).
 - [6] P. Manshour, S. Saberi, M. Sahimi, J. Peinke, A. F. Pacheco, and M. R. Rahimi Tabar, *Phys. Rev. Lett.* **102**, 014101 (2009).
 - [7] S. Ghashghaie, W. Breymann, J. Peinke, P. Talkner, and Y. Dodge, *Nature (London)* **381**, 767 (1996).
 - [8] R. N. Mantegna and H. E. Stanley, *Nature (London)* **383**, 587 (1996).
 - [9] A. Hilgers and C. Beck, *Int. J. Bifurcat. Chaos* **07**, 1855 (1997).
 - [10] A. Arnéodo, J. F. Muzy, and D. Sornette, *Eur. Phys. J. B* **2**, 277 (1998).
 - [11] W. Breymann, S. Ghashghaie, and P. Talkner, *Int. J. Theor. Appl. Finan.* **03**, 357 (2000).
 - [12] T. Lux, *Quant. Finance* **1**, 632 (2001).
 - [13] U. A. Müller, M. M. Dacorogna, R. D. Davé, R. B. Olsen, O. V. Pictet, and J. E. von Weizsäcker, *J. Empir. Finance* **4**, 213 (1997).
 - [14] R. Gençay, N. Gradojevic, F. Selçuk, and B. Whitcher, *Quant. Finance* **10**, 895 (2010).
 - [15] A. M. S. Macêdo, Ivan R. R. González, D. S. P. Salazar, and G. L. Vasconcelos, *Phys. Rev. E* **95**, 032315 (2017).
 - [16] A. Chaboud, D. Rime, and V. Sushko, *Research Handbook of Financial Markets*, edited by R. S. Gurkaynak and J. H. Wright (Edward Elgar, Cheltenham, UK, 2023), chap. 12
 - [17] The data were downloaded from the historical center of the MetaTrader 4 platform.
 - [18] D. S. P. Salazar and G. L. Vasconcelos, *Phys. Rev. E* **82**, 047301 (2010).
 - [19] D. S. P. Salazar and G. L. Vasconcelos, *Phys. Rev. E* **86**, 050103(R) (2012).
 - [20] N. Shephard and T. G. Andersen, *Handbook of Financial Time Series*, edited by T. Mikosch, J.-P. Kreiß, R. A. Davis, and T. G. Andersen (Springer, Berlin, 2009), pp. 233–254.
 - [21] B. Mandelbrot, *J. Bus.* **40**, 393 (1967).
 - [22] M. M. Dacorogna, U. A. Muller, O. V. Pictet, and R. B. Olsen, *Nonlinear Modelling of High Frequency Financial Time Series*, edited by C. Dunis and B. Zhou (John Wiley & Sons, New York, 1998), pp. 161–176.
 - [23] R. Cont, *Quant. Finance* **1**, 223 (2001).
 - [24] J.-P. Bouchaud, A. Matacz, and M. Potters, *Phys. Rev. Lett.* **87**, 228701 (2001).
 - [25] A. Erdélyi, W. Magnus, F. Oberhettinger, and F. G. Tricomi, in *Higher Transcendental Functions* (McGraw–Hill, New York, 1953).
 - [26] C. Tsallis, *J. Statist. Phys.* **52**, 479 (1988).
 - [27] C. Tsallis, *Introduction to Nonextensive Statistical Mechanics: Approaching a Complex World* (Springer, New York, 2009).

- [28] G. L. Vasconcelos, D. S. P. Salazar, and A. M. S. Macêdo, *Phys. Rev. E* **97**, 022104 (2018).
- [29] W. Sosa-Correa, R. M. Pereira, A. M. S. Macêdo, E. P. Raposo, D. S. P. Salazar, and G. L. Vasconcelos, *Phys. Rev. Fluids* **4**, 064602 (2019).
- [30] The concept of information cascade used here is different from the notion of “informational cascade” in economic and social theory, whereby a cascade occurs when a person ignores their own private information and makes a decision based on decisions by other people, see, e.g., Ref. [36], for a review on this topic.
- [31] A. Kartono, M. Febriyanti, S. T. Wahyudi, and Irmansyah, *Physica A: Stat. Mech. Appl.* **560**, 125191 (2020).
- [32] E. Bacry, A. Kozhemyak, and J.-F. Muzy, *J. Econ. Dynam. Contr.* **32**, 156 (2008).
- [33] J.-i. Maskawa and K. Kuroda, *Front. Phys.* **8**, 565372 (2020).
- [34] H. Hong and J. C. Stein, *Rev. Financ. Stud.* **16**, 487 (2003).
- [35] S. L. Braunstein, M. Faizal, L. M. Krauss, F. Marino, and N. A. Shah, *Nat. Rev. Phys.* **5**, 612 (2023).
- [36] S. Bikhchandani, D. Hirshleifer, O. Tamuz, and I. Welch, *Information Cascades and Social Learning*, Working Paper 28887 (National Bureau of Economic Research, 2021).